

WATER FORMATION THROUGH A QUANTUM TUNNELING SURFACE REACTION, OH + H₂, AT 10 K

Y. Oba, N. Watanabe, T. Hama, K. Kuwahata, H. Hidaka, and A. Kouchi

*Institute of Low Temperature Science, Hokkaido University, Sapporo, Hokkaido 060-0819,
Japan*

oba@lowtem.hokudai.ac.jp

ABSTRACT

The present study experimentally demonstrated that solid H₂O is formed through the surface reaction OH + H₂ at 10 K. This is the first experimental evidence of solid H₂O formation using hydrogen in its molecular form at temperatures as low as 10 K. We further found that H₂O formation through the reaction OH + H₂ is about one order of magnitude more effective than HDO formation through the reaction OH + D₂. This significant isotope effect results from differences in the effective mass of each reaction, indicating that the reactions proceed through quantum tunneling.

Subject headings: astrobiology – astrochemistry – atomic processes – ISM: clouds – ISM: molecules

1. Introduction

1.1. H₂O formation

Water (H₂O) is the most abundant solid component of icy grain mantles in molecular clouds. Previous theoretical studies demonstrated that the observed abundance of solid H₂O in molecular clouds cannot be explained by gas-phase synthesis alone (e.g. Hasegawa et al. 1992). Therefore, H₂O is mainly considered to be formed on the surfaces of interstellar grains. Tielens & Hagen (1982) proposed a chemical reaction network by which the formation of solid H₂O begins with hydrogenation of O atoms, O₂, or ozone, O₃, on the grain surfaces. Since this proposal, many researchers have experimentally explored possible pathways for

the formation of solid H₂O under the simulative conditions of dense molecular clouds. These studies showed that solid H₂O is produced through various surface reactions at temperatures as low as 10 K. The main surface reactions leading to the formation of solid H₂O and some related to H₂O formation are listed in Table 1.

The simplest pathway toward the formation of solid H₂O is the sequential hydrogenation of O atoms:



Cuppen & Herbst (2007) proposed that reaction (2) is the main route toward H₂O formation in diffuse and translucent clouds in which H atoms are more prevalent than H₂ molecules. Several groups have experimentally approached these reactions using D atoms instead of H atoms. For example, Hiraoka et al. (1998) sprayed D atoms over O atoms trapped in an N₂O matrix at 12 K. The O and D atoms were produced by dissociation of, respectively, N₂O and D₂ under a dc discharge. Dulieu et al. (2010) codeposited O and D atoms produced by dissociating O₂ and D₂, respectively, onto non-porous amorphous H₂O ice at 10 K. More recently, Jing et al. (2011) deposited D atoms and ¹⁸O (instead of ¹⁶O) at 15–25 K on a synthesized olivine surface. All three groups claimed that D₂O (HDO) formed during their experiments through surface reactions (1) and (2); however, other O-related species, such as O₂ and O₃, were also present in or on the samples, and it was difficult to separate information relating to reactions (1) and (2) from the different competing H₂O-formation channels related to O₂ and O₃, shown below. Further studies are desired to isolate these reactions (1) and (2) from reactions involving species other than H and O.

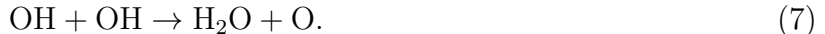
The second simplest formation pathway involves the sequential hydrogenation of O₂ via the formation of hydrogen peroxide (H₂O₂):



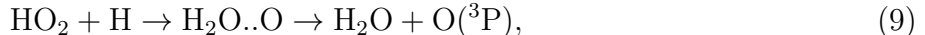
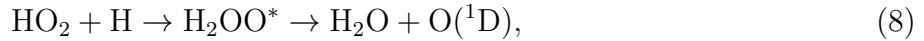
Miyauchi et al. (2008) first revealed experimentally that these reactions proceed at 10 K and that a significant isotope effect is apparent for reaction (5) but not for reactions (3) and (4). This is consistent with the fact that reactions (3) and (4) have essentially no barrier (Walch et al. 1988; Sellevag et al. 2008), whereas reaction (5) has a significant barrier of about 2000 K (Koussa et al. 2006) and requires quantum tunneling (Miyauchi et al. 2008).

After the experimental study by Miyauchi et al. (2008), extensive studies were performed on the hydrogenation of O₂ at low temperatures. Ioppolo et al. (2008) revealed that

reactions (3)–(5) occur even at 28 K. Furthermore, it was found that the structure of the H₂O ice formed through reactions (3)–(5) is amorphous (Oba et al. 2009), which is consistent with the astronomical observations (Smith et al. 1989). The recent detection of H₂O₂ in the cloud core of ρ Oph A further supported the occurrence of these reactions on the surface of interstellar grains (Bergman et al. 2011) because gas-phase synthesis of H₂O₂ through reactions (3) and (4) is not favored (Mousavipour & Saheb 2007). In the gas phase, H₂O₂ formed through reaction (4) further dissociates into two OH species using the excess energy from H₂O₂ formation (Mousavipour & Saheb 2007). In the solid phase, the release of the excess energy from reaction (4) into the cold surface will stabilize the formed H₂O₂ on the surface. Even though the dissociation occurs, OH radicals are expected to recombine, resulting in the recovery of H₂O₂ (reaction (6)) and/or the formation of H₂O (reaction (7)), as follows:



The reaction HO₂ + H in the gas phase was theoretically predicted to follow two channels to produce H₂O via an intermediate species as follows:



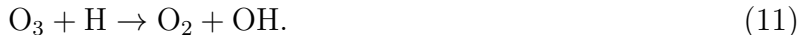
where H₂OO* and H₂O..O denote short-lived intermediate species (Mousavipour & Saheb 2007). Reaction channel (8) as a whole is slightly exothermic by 10 kJ mol⁻¹, whereas the latter part of the reaction (H₂OO* → H₂O + O(¹D)) is highly endothermic by 151 kJ mol⁻¹ (Mousavipour & Saheb 2007), indicating that reaction channel (8) would not go to completion if the intermediate H₂OO* dissipated the excess energy to a cold surface. Reaction (9) has a huge barrier of about 9300 K, implying that the reaction proceeds only with difficulty, even with tunneling under astrophysically relevant conditions. Furthermore, the branching ratio to produce O atom is only 2% for reaction of HO₂ + H in the gas phase (Keyser 1986). Although Cuppen et al. (2010) claimed that the reaction HO₂ + H → H₂O + O occurred in their O₂/H codeposition experiments, this reaction would be unlikely in the present experiment.

Reactions of HO₂ with H may also lead to the formation of H₂ and O₂(³Σ_g⁻) (Mousavipour & Saheb 2007):



In the gas phase, this reaction occurs much less frequently than reaction (4) (Keyser 1986). Even if O₂ were reproduced through reaction (10), it must be hydrogenated once again to yield HO₂ and finally H₂O₂ like in the O₂-hydrogenation experiments.

The sequential hydrogenation of ozone (O_3) may occur in molecular clouds:



The products (O_2 and OH) may be further used for H_2O formation. Mokrane et al. (2009) investigated these reactions at 10 K by irradiating solid O_3 on H_2O ice with D atoms. The reaction products were analyzed using temperature-programmed desorption (TPD) methods. Romanzin et al. (2011) performed experiments of the hydrogenation of O_3 at higher temperatures (25, 40, and 50 K), and the reaction products were monitored in-situ by Fourier-transform infrared (FTIR) spectroscopy. Both studies provided results indicating that the formation of H_2O was initiated by reaction (11).

Note that OH is always produced along each of these three pathways: reaction (1) for the hydrogenation of O atoms, reaction (5) for that of O_2 , and reaction (11) for that of O_3 . Hence, in addition to the H-atom related reactions shown above, the following H_2 -related reaction would lead to H_2O formation:



which has an activation barrier of ~ 2100 K in the gas phase (Atkinson et al. 2004). Despite the large activation barrier of reaction (12), reaction (12) is often thought of as the most common route to the formation of H_2O on grain surfaces in dense molecular clouds in which typical temperatures are about 10 K, the UV flux is very low, and H_2 is the dominant H-bearing species over H atoms (Tielens & Hagen 1982; Tielens 2005; Cuppen & Herbst 2007). At temperatures as low as 10 K, Arrhenius-type reactions having an activation barrier of ~ 2000 K occur only rarely. Therefore, reaction (12) requires quantum tunneling to proceed on grain surfaces, as observed in the gas-phase reaction at low temperatures (Nguyen et al. 2011). The tunneling reaction is described in further detail in the next section.

Reaction (12) was experimentally studied in the gas phase (Ravishankara et al. 1981; Oldenberg et al. 1992; Alagia et al. 1993; Talukdar et al. 1996; Krasnoperov & Michael 2004; Orkin et al. 2006). In most previous studies, OH was produced by photolysis of H_2O or H_2O_2 , or indirectly by photolysis of N_2O to generate $\text{O}(^1\text{D})$ atoms, which further reacted with H_2O (Vaghjiani et al. 1989; Oldenberg et al. 1992; Talukdar et al. 1996; Orkin et al. 2006). OH generated through those energetic processes should have significant excess energy that should be sufficient to overcome the activation barrier of reaction (12). Hence, to investigate whether reaction (12) occurs through quantum tunneling on cold grains, non-energetic OH must be used for experiments. In recent experimental studies of low-temperature surface reactions, OH radicals were produced through various reactions and were further used in secondary reactions. For example, hydrogenation of O_3 yielded OH as a reaction product (reaction (11)); however, OH formed in reaction (11) could be highly energetic because the heat of the

reaction ($\sim 39,000$ K; Keyser 1979) is partitioned into OH (Romanzin et al. 2011), which is not suitable for investigating quantum tunneling reactions.

We recently succeeded in producing cold OH by dissociating H₂O in a microwave-induced plasma, followed by cooling to 100 K before reaching the reaction substrate (Oba et al. 2010a,b, 2011). A similar technique for producing OH in the electronic and vibrational ground states was applied to crossed beam studies of reaction (12) in the gas phase (Alagia et al. 1993), where OH was produced in a radiofrequency-induced H₂O plasma. We found that the cold OH can react with CO and HOCO on a substrate even at 10 K to yield CO₂ (Oba et al. 2010a) and H₂CO₃ (Oba et al. 2010b), respectively. Moreover, it was experimentally demonstrated that cold OH reacts with another OH to yield H₂O₂ and H₂O through reactions (6) and (7), respectively, even at 40 K (Oba et al. 2011). Consequently, our experimental method is useful for studying chemical reactions related to cold OH on the surfaces of interstellar grain mantles.

In the present study, we first performed the codeposition of cold OH with H₂ on a cold substrate to study reaction (12) as a possible route to the formation of H₂O on the surfaces of interstellar grains in dense molecular clouds. Next, OH and/or H₂ isotopologues, such as OD and D₂, were studied experimentally in an investigation of the isotope effect on the reactions to decisively conclude that these reactions occur via quantum tunneling.

1.2. Quantum tunneling reaction

The thermally activated reaction (12) is not expected to occur on grain surfaces at 10 K for the reasons given above. Previous experimental and theoretical studies proposed that quantum tunneling plays a significant role in reaction (12) in the gas phase, particularly at low temperatures (e.g. Talukdar et al. 1996; Nguyen et al. 2011). Watanabe & Kouchi (2008) described the importance of quantum tunneling in various chemical reactions on low-temperature grain surfaces in molecular clouds. Under the simple assumption that a reaction occurs through a rectangular barrier of height E_a and width a on a potential energy surface, the rate of a quantum tunneling reaction (k_q) is approximately represented by the following equation:

$$k_q \approx v_0 \exp\left[-\left(\frac{2a}{\hbar}\right)(2mE_a)^{\frac{1}{2}}\right], \quad (13)$$

where v_0 and m denote the frequency of harmonic motion and particle mass, respectively. In the case of a bimolecular atom-transfer reaction represented by $A + XB \rightarrow AX + B$, the center of mass translated from the initial state ($A + XB$) to the final state ($AX + B$) of a reaction on the potential energy surface is represented as the effective mass m_c which is

defined by the following equation:

$$m_c = \frac{m_a m_b (1 + c)^2 + m_b m_x c^2 + m_a m_x}{M(1 + c^2)}, \quad (14)$$

where m_a , m_x , and m_b are the masses of A, X, and B atoms, respectively, M is the mass of the linear triatomic molecule AXB ($M = m_a + m_x + m_b$), and c is the ratio of the infinitesimal change of one bond distance to that of the other bond distance (Johnston 1966). When bimolecular atom-transfer reactions $A + XB \rightarrow AX + B$ proceed through quantum tunneling, an effective mass m_c should be used to indicate the tunneling mass in Equation (13) (Hidaka et al. 2009).

Observation of an isotope effect on a reaction can be an indicator of quantum tunneling. This is because tunneling effects strongly depend on the particle mass, such that a tunneling reaction involving a species with a lighter effective mass proceeds faster than with a heavier effective mass. Previous studies have investigated the isotope effect on other astrophysically relevant chemical reactions around 10 K. Hidaka et al. (2007) performed hydrogenation/deuteration of solid CO at 10–20 K and found that hydrogenation of CO proceeds faster than deuteration of CO by a factor of about 12. H–D isotope exchange reactions of methanol (CH_3OH) were also demonstrated to occur through quantum tunneling (Nagaoka et al. 2007), which would contribute to the observed abundance of deuterated methanol, such as CHD_2OH .

The importance of the effective mass on quantum tunneling reactions has been demonstrated experimentally. Hidaka et al. (2009) extensively investigated H-D exchange reactions of formaldehyde (H_2CO) at 10–20 K. The effective mass of the D-atom abstraction by H atoms from D_2CO is ~ 1 , whereas that of the H-atom abstraction by D atoms from H_2CO is ~ 0.5 , which affects the rate of each reaction (Hidaka et al. 2009).

Most quantum tunneling surface reactions previously studied were H- and D-atom-related reactions. Previous experimental studies of H_2 -related quantum tunneling reactions have investigated the isotope effect on the reactions of methyl radicals (CH_3) or its deuterated species (e.g. CHD_2 and CD_3) in solid parahydrogen ($E_a \sim 5300$ K) at 5 K (Momose et al. 1998; Hoshina et al. 2004). Although these pioneering studies are important for understanding quantum tunneling reactions related to H_2 , their relevance to astrophysics is rather weak because their experiments were conducted under unfeasible conditions (in a parahydrogen matrix at 5 K) in molecular clouds.

In the present study, we experimentally examined surface reactions related to H_2 and OH isotopologues, as shown below, to investigate the isotope effects on reaction (12):





The use of isotopically substituted hydrogen (HD or D₂) or hydroxyl radical (OD) in place of H₂ or OH, respectively, can alter the effective mass of a reaction relative to that of reaction (12). In this case, the rate of a quantum tunneling reaction should differ from that of reaction (12) as well. Reported values of the activation barrier and the calculated effective mass for each reaction are summarized in Table 2. According to Hidaka et al. (2009), the value of c in Equation (14) was set to -1 in the present reaction system. An observation that the efficiency of each reaction varied according to the effective mass would strongly indicate that these reactions proceed through quantum tunneling.

2. EXPERIMENTAL

2.1. Apparatus and experimental conditions for the surface reactions

Experiments were performed using the Apparatus for SURface Reaction in Astrophysics system. Details of this apparatus and experimental conditions have been described previously (Watanabe et al. 2006; Nagaoka et al. 2007; Oba et al. 2010a, 2011). Briefly, OH radicals, together with H atoms, were produced by the dissociation of H₂O in a microwave discharge plasma (Timmermans et al. 1998, 1999) in a Pyrex tube. H₂O dissociation can lead directly to the formation of H₂ and O. The species produced in the OH source are denoted “H₂O fragments” in this paper. H₂O fragments were transferred via a series of poly(tetrafluoroethylene) and a cold aluminum (Al) tube, which was connected to a He refrigerator, and they impinged on the substrate. Initially, OH radicals may be excited when formed in the plasma, but after many collisions with the inner wall of a cold Al pipe, they are thermalized to 100 K. That is, they should be vibrationally and electronically in the ground state before reacting on the substrate, as demonstrated in gas-phase collision experiments (Alagia et al. 1993; Kohno et al. 2011). This was confirmed experimentally, as described in the next section. The deposition rate of OH radicals was not measured directly; the upper limit of the deposition rate should be 1.5×10^{13} radicals cm⁻² s⁻¹, which is equal to the deposition rate of H₂O when the microwave source is turned off. H₂ molecules delivered from a separate gas line through a capillary plate were codeposited with the H₂O fragments onto

the substrate over 60 minutes. The flux of H_2 was calculated to be 2.0×10^{14} molecules $\text{cm}^{-2} \text{s}^{-1}$ based on the measured pressure inside the main chamber when filled with only H_2 .

The reaction products were monitored in-situ by reflection-absorption-type FTIR with a resolution of 4 cm^{-1} in the spectral range $4000\text{--}800 \text{ cm}^{-1}$. The desorbed species from the substrate were monitored using a quadrupole mass spectrometer (QMS). The temperature of the substrate, which was connected to another He refrigerator, was kept at 10 K in each experiment. The reactions in Table 2 did not occur if the codeposition experiments were performed at temperatures above 20 K.

After codeposition, the TPD spectra were obtained by the QMS at a heating rate of 4 K minutes^{-1} .

In the experiments using H_2 - and OH-isotopologues, the HD and D_2 fluxes were the same as the H_2 flux. QMS measurements and a resonance-enhanced multiphoton ionization (REMPI) method (see Section 2.2) confirmed that almost all ($>95\%$) D_2O or H_2O introduced into the radical source was fragmented when the microwave source was turned on. On this basis, the deposition rate of OD was considered to be similar to that of OH because the flow rates of D_2O and H_2O into the radical source were adjusted to the same value.

2.2. In Situ Detection of OH Radicals

The direct detection of OH from the source was performed using another apparatus, named RASCAL, in our laboratory. RASCAL is described in detail elsewhere (Watanabe et al. 2010; Hama et al. 2011). OH from the radical source was selectively ionized by $(2 + 1)$ REMPI approximately 5 mm from the exit of the aluminum pipe and detected using a time-of-flight mass spectrometer.

Figure 1(a) shows the REMPI spectrum of $\text{OH}(v=0)$ via the $D^2\Sigma^-(v'=0) \leftarrow X^2\Pi(v=0)$ transition under conditions in which the Al pipe was equilibrated at room temperature. The presence of vibrationally excited $\text{OH}(v=1)$ was sought using the REMPI, with $3^2\Sigma^-(v'=0) \leftarrow X^2\Pi(v=1)$ transition; however, no such evidence was obtained. Greenslade et al. (2005) calculated that the two-photon cross-sections of the $D^2\Sigma^-(v' = 0) \leftarrow X^2\Pi(v=0)$ and $3^2\Sigma^-(v' = 0) \leftarrow X^2\Pi(v=1)$ transitions are comparable; therefore, the present results indicate that OH from the radical source was electronically and vibrationally in the ground state. The REMPI spectrum of $\text{OH}(v=0)$ was assigned and modeled using the PGOPHER simulation program to determine the rotational structure (C. M. Western, available from <http://pgopher.chm.bris.ac.uk>). The constants associated with the relevant electronic states were compared with those in the literature (Dieke & Crosswhite 1962; Greenslade et al. 2005;

Huber & Herzberg 1979). Figure 1(b) shows the results of a spectral simulation of OH($v=0$) assuming a rotational temperature of 300 K. By comparison with the spectral simulation, the OH($v=0$) from the radical source was expected to be almost thermally equilibrated with the Al pipe before reacting on the substrate.

In an additional step, the adsorbates were photodesorbed using the weak second harmonic radiation (532 nm) of a Nd:YAG laser and were analyzed by the REMPI method. We detected OH($v=0$) signals in the species photodesorbed from the cold substrate (10–40 K) during the deposition of H₂O fragments. Photolysis of H₂O or H₂O₂ on the substrate, which could be potential sources for OH($v=0$), was negligible at 532 nm (Chu & Anastasio 2005; Kobayashi 1983); therefore, this result clearly indicates the presence of OH in the electronic and vibrational ground states on the substrate at 10 K. The rotational temperature of the photodesorbed OH($v=0$) was about 100 K. This value is slightly higher than the substrate temperature. The OH radical is considered to gain a small amount of energy during photo-stimulated desorption. The present results are consistent with previous experimental results obtained using a similar method at 3.5 K (Zins et al. 2011).

3. RESULTS AND DISCUSSION

3.1. OH + H₂

The deposition only of H₂O fragments on a substrate at 10 K resulted in the formation of H₂O, H₂O₂, and O₃, as identified in the product IR spectrum at 1650, 1400, and 1040 cm⁻¹, respectively (Figure 2(a)). Hereafter, this experiment is denoted as the H₂O-fragment deposition. In contrast, these molecules were not observed in the H₂O-fragment deposition at 60 K (Oba et al. 2011). If H₂O, H₂O₂, and O₃ formed in the gas phase, they should be adsorbed on the substrate even at 60 K, which is well below their desorption temperatures. We therefore concluded that these molecules were formed through surface reactions at 10 K. The formation pathways of these molecules are described in our recent paper (Oba et al. 2011). The peak area for each reaction product increased linearly with the deposition time. In addition to the three types of molecules listed above, QMS measurements revealed that H₂ and O₂, which are infrared-inactive, are present in the gases from the source and/or are produced on the surface.

Figure 2(b) shows the IR spectrum of the reaction product obtained after codeposition of H₂O fragments with H₂. This spectrum was obtained under the same experimental conditions as those for the H₂O-fragment deposition: the deposition rate of OH, the experimental time, and substrate temperatures. The resulting spectrum was similar to that obtained in the

H₂O-fragment deposition, although the peak area associated with the OH bending of H₂O (1650 cm⁻¹) increased by a factor of two compared to that observed in the H₂O-fragment deposition (Figure 2(c)). This result indicates that the introduced H₂ was used for the formation of H₂O through surface reactions with O-related species, such as OH, O, O₂, and/or O₃. We concluded that H₂O was formed by reaction of H₂ with OH (reaction (12)) on the surface at 10 K, despite the relatively large barrier E_a of about 2100 K (Atkinson et al. 2004), for the following reasons.

First, we confirmed that codeposition of H₂ with cold O atoms produced by the dissociation of O₂ in a microwave-induced plasma did not result in a reaction at 10 K, except that O₃ formed (Y. Oba et al., unpublished data). This result indicates that cold O atoms in an H₂O plasma will not react with H₂ either. This is in good agreement with the fact that the reaction,



is endothermic by 8 kJ mol⁻¹ (= 960 K) with a significant activation barrier of 3160 K (Baulch et al. 1992), although theoretical studies assumed H₂O formation begins with reaction (22) (Cazaux et al. 2010, 2011). Second, O₂ never reacts with H₂ under the present experimental conditions. Third, O₃ does not react with H₂, as experimentally demonstrated previously (Mokrane et al. 2009; Romanzin et al. 2011). In addition, if HO₂ is produced through reactions of the H₂O fragments, it may react with H₂ to yield H₂O₂:



In this case, the H₂O₂ produced may further yield H₂O through reaction (5). This, however, is unlikely in the present experiment because reaction (23) is highly endothermic with a considerable activation barrier (Table 1).

The column density of the H₂O product was calculated from the peak area of the OH bending band at 1650 cm⁻¹ and the previously reported integrated band strengths, as described in Hidaka et al. (2007). The band strength used was 1.2×10^{-17} cm molecules⁻¹ which is by a transmission method (Gerakines et al. 1995). We confirmed that the ratio of the band strengths for OH stretching and bending bands of H₂O is almost independent of the method (transmission or reflection). While, the difference in the absolute value of band strengths for the reflection and the transmission methods was found to be within the factor of two in our experimental setup (Hidaka et al. 2009). Moreover, it is difficult to determine the exact column density even by the transmission method in the layered and the mixed samples. However, since our discussion is based on relative reaction yields, the difference in the absolute value of the band strengths between the two methods little alters the present experimental results and discussion.

By subtracting the H₂O band obtained in the H₂O-fragment deposition from that obtained in the codeposition experiment, we determined the increase in the column density of H₂O through reaction (12) to be 3.5×10^{15} molecules cm⁻². Note that it is not obvious whether H₂O yield obtained by the subtraction gives the total yield of H₂O by the reaction OH + H₂. In the H₂O-fragment deposition, two competing reactions produce H₂O: reactions (7) and (12). In the codeposition experiment, additional H₂ molecules enhance reaction (12). That is, a part of OH amount which was used by reaction (7) in the H₂O-fragment deposition may be consumed by reaction (12). Therefore, H₂O column density obtained by the subtraction may be underestimated compared to the total yield of H₂O by reaction (12) in the codeposition. Further details on this issue are shown in the next section.

Accompanied by the increase in the H₂O column density, the peak area of the OH bending in H₂O₂ at 1400 cm⁻¹ decreased relative to the peak area measured in the H₂O-fragment deposition (Figure 2(c)). This is probably because the abundant H₂ which was codeposited with H₂O fragments inhibited the formation of H₂O₂ through reaction (6) (OH + OH → H₂O₂); the OH fragments instead formed H₂O via reaction (12). Reaction (2) (OH + H → H₂O) was assumed to contribute to H₂O formation only to a minor extent in the present study because most H atoms in the H₂O fragments must be consumed by H–H recombination on the surface or few H atoms were present in the gases from the source. In fact, the codeposition of O₂ with the H₂O fragments did not increase the amount of H₂O₂ relative to the H₂O-fragment deposition, despite the barrierless mechanism for O₂ hydrogenation.

The absorption at 1040 cm⁻¹ due to O₃ was not observed in the codeposition experiment (Figure 2(b)). It is possible that O₃ was consumed by H atoms (reaction (11)) that formed through reaction (12) and/or the O atoms were similarly consumed by H atoms (reaction (1)) prior to the formation of O₃ (O₂ + O → O₃). Reactions (1) and (11) yield energetic OH, which may further react with H₂ to yield H₂O through reaction (12). Even if this were the case, the low O₃ column density produced in the H₂O-fragment deposition (0.6×10^{15} molecules cm⁻²) suggested that such reactions did not significantly contribute to the observed H₂O column density. Nevertheless, a lack of O₃ could provide indirect evidence that the reaction OH + H₂ occurred. In fact, the codeposition of D atoms with H₂O fragments did not yield O₃ formation (see Section 3.3).

3.2. OD + H₂

Similar experiments were performed using OD instead of OH. If OD reacts with H₂, the formation of HDO is expected to occur through the following H-atom abstraction from H₂

by OD:



which has almost the same activation barrier and effective mass as reaction (12) (Nguyen et al. 2011, Table 2). In the OH/H₂ codeposition experiment described in the previous section, the reaction products were basically the same as those of the H₂O-fragment deposition except for the presence of O₃. In contrast, HDO, the reaction product of reaction (15), is not produced unless both H and D-related species are used, that is, HDO is never produced in the deposition only of H₂O or D₂O fragments. The formation of HDO should thus provide direct evidence that reaction (15) occurs at 10 K.

Formation of D₂O, D₂O₂, and O₃ was observed in the product IR spectrum upon the sole deposition at 10 K of D₂O fragments (Figure 3(a)) (hereafter, this experiment is denoted as the D₂O-fragment deposition), which were produced in a manner similar to that used to produce H₂O fragments. These results indicated that the isotopic substitution of H₂O fragments did not significantly alter the reaction pathways on the cold substrate.

The codeposition of D₂O fragments with H₂ resulted in the appearance of new peaks at 3392, 2858, and 1453 cm⁻¹ (Figure 3(b)). Absorption bands at 3392 and 1453 cm⁻¹ were typically observed for solid HDO produced by depositing an H₂O and D₂O mixture on a substrate at 100 K or lower (Hornig et al. 1958; Devlin et al. 1986; Gálvez et al. 2011). The absorption band at 2858 cm⁻¹ may correspond to the 2*v*₂ vibration of HDO (Devlin et al. 1986). Because the only H source is H₂ and other O-related species, such as O atoms and O₃, hardly react with H₂, as explained in Section 3.1, we conclude that H₂ reacted with OD to yield HDO on the surface at 10 K. The presence of HDO in the reaction product was also confirmed by the TPD experimental results. Figure 4 shows the integrated TPD yields of *m/z* = 19 (HDO) plotted with the peak area of the band at 1453 cm⁻¹.

The column density of HDO was calculated from the peak area of the OH-stretching band, and the previously reported integrated band strength of 1.3×10^{-16} cm molecule⁻¹ for the OH-stretching band of the solid HDO (Ikawa & Maeda 1968) was found to be 4.7×10^{15} molecules cm⁻².

In contrast to the experimental result shown in the previous section, the obtained column density of HDO should represent the total yield of HDO by the reaction OD + H₂ because HDO is not formed in the D₂O-fragment deposition. The HDO yield is very similar to the estimated yield of H₂O by the reaction OH + H₂ (3.5×10^{15} molecules cm⁻²) in the previous section. It is reasonably considered that our estimated H₂O yield represents the total yield of H₂O by the reaction OH + H₂. This is based on an assumption that reaction (12) has the same efficiency with reaction (15) (see Section 3.6 for further details).

3.3. OH + D₂

We next codeposited H₂O fragments with D₂ to investigate the efficiency of reaction (16), which had almost the same barrier as reactions (12) and (15) in the gas phase (Nguyen et al. 2011). The effective mass of reaction (16) was twice that of reactions (12) and (15) (Table 2). Figure 5 shows an IR spectrum of the reaction product obtained after codeposition of H₂O fragments with D₂. The spectrum resembled that obtained from the H₂O-fragment deposition (Figure 2(a)); however, a broad peak grew in at 2475 cm⁻¹, which is a typical position for OD-stretching bands. In addition, a small peak was observed at 2150 cm⁻¹. This peak may be associated with D₂O₂ (Lannon et al. 1971), which is probably produced through deuteration of O₂ by the D atoms formed through reaction (16). Because the only D source is D₂ in this experiment, the appearance of an OD-stretching band indicates that reaction (16) occurred at 10 K. The presence of HDO was verified in the TPD experiment.

The column density of the formed HDO was calculated based on the peak area of the OD stretching band at 2475 cm⁻¹ and the previously reported integrated band strengths of 5.0×10^{-17} cm molecule⁻¹ for the OD stretching band of the solid HDO (Ikawa & Maeda 1968). The column density was found to be 2.7×10^{14} molecules cm⁻², much lower than the column density of the H₂O formed via reaction (12) under the similar experimental conditions (see Section 3.1). A low efficiency was also inferred from the presence of O₃ in the reaction product (Figure 5). As described above, if reaction (16) proceeds efficiently to produce significant quantities of D atoms, O₃ would be consumed. In fact, the codeposition of H₂O fragments with D atoms did not result in observation of O₃.

3.4. OD + D₂

Reactions of OD with D₂ are expected to yield D₂O and D atoms as follows:



Because the effective mass for reaction (17) exceeds those of reactions (12) and (15) and is comparable to that of reaction (16), reaction (17) is expected to be less efficient than reactions (12) and (15). Figure 6 shows an IR spectrum obtained after codeposition of D₂O fragments with D₂. The spectrum resembled that of the D₂O-fragment deposition (Figure 3(a)). A slight increase in the OD bending band of D₂O was observed at 1200 cm⁻¹, which corresponds to an increase in the D₂O column density by 3.5×10^{14} molecules cm⁻². The band strength used was 8.0×10^{-18} cm molecule⁻¹ (Miyachi et al. 2008).

3.5. OH or OD + HD

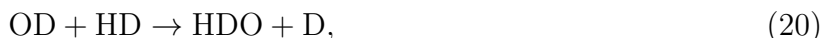
Unlike reactions that involve H₂ or D₂, two reaction channels are available for OH in the presence of HD:



These reactions are associated with nearly identical barrier heights (Nguyen et al. 2011) whereas the effective masses differed considerably from one another (0.48 for reaction (18) and 0.90 for reaction (19)). The experimental results shown in Sections 3.1–3.4, therefore, predict that reaction (18) is more efficient than reaction (19). The branching ratio for these reactions in the gas phase was experimentally estimated, suggesting that reaction (18) was 3–4 times more efficient than reaction (19) (Talukdar et al. 1996). H₂O fragments were codeposited with HD to investigate the efficiencies of reactions (18) and (19).

The formation of H₂O and H₂O₂ was observed in the product IR spectrum obtained after codeposition of H₂O fragments with HD. O₃ was not observed (Figure 7(a)). The peak area for H₂O increased by a factor of 1.5 compared to the H₂O-fragment deposition (Figure 7(b)), which corresponded to an increase in the H₂O column density by 3.1×10^{15} molecules cm⁻². In addition to the H₂O increase, small peaks were observed at 2435 and 2114 cm⁻¹ (Figure 7(b)). The former peak corresponded to an OD-stretching band, implying that HDO was formed through the reaction OH + HD; however, the observed OD-stretching band was expected to include large contributions from species other than HDO. If reaction (18) is the dominant channel relative to reaction (19), D atoms are produced together with H₂O, which results in the formation of D₂O₂ through reactions between D and O₂ contained in the H₂O fragments. In fact, the peak positions at 2435 and 2114 cm⁻¹ were consistent with D₂O₂ (Lannon et al. 1971). Assuming that the OD-stretching band was mainly derived from D₂O₂, the contributions of HDO to the band should be very small.

As with the reaction OH + HD, two reaction channels were possible for the reactions of OD with HD:



For the reasons mentioned above, reaction (20) was expected to be more efficient than reaction (21). Figure 8(a) shows an IR spectrum of the reaction product obtained after codeposition of D₂O fragments with HD. Several new peaks were observed, most of which corresponded to HDO, as explained earlier. The column density of HDO was estimated from the OH-stretching band at 3400 cm⁻¹ to be 3.3×10^{15} molecules cm⁻².

In contrast, the column density of D₂O did not increase; rather, it decreased upon codeposition, as indicated by the decrease in peak area derived from the OD-bending band for D₂O at 1200 cm⁻¹ (Figure 8(b)). This result indicated that reaction (21) is not effective. Assuming that D₂O was mainly produced through OD + OD → D₂O + O in the D₂O-fragment deposition, the decrease in the D₂O column density upon codeposition was mainly attributed to consumption of the corresponding OD by HD through reaction (20). This was based on the fact that reaction (17) (OD + D₂ → D₂O + D) was not efficient, as demonstrated in Section 3.4. D₂O₂ was assumed to form via the reaction OD + OD, and it may be consumed in the presence of codeposited HD; however, variations in the D₂O₂ column density could not be estimated because the OD bending band of D₂O₂ at 1000 cm⁻¹ mixed with the bands corresponding to other species, such as O₃ (Figure 8(b)).

3.6. Relative reaction efficiency

We found that H₂O and its isotopologues (HDO and D₂O) form through surface reactions of OH or OD with H₂, HD, or D₂ at 10 K, and we determined the column densities of the reaction products in previous sections (Sections 3.1–3.5). The relative efficiency of each reaction was roughly estimated by comparing the column densities of the reaction products obtained under identical conditions (Table 2). More accurate relative efficiencies, however, could not be obtained due to the reason shown below. As indicated in Section 2.1, the accurate fluxes of OH or OD were not measured experimentally, just assigned an upper limit of 1.5×10^{13} radicals cm⁻² s⁻¹, which is equal to the deposition rate of H₂O or D₂O when the microwave source is turned off. Although we verified by QMS and REMPI that almost all H₂O and D₂O molecules were fragmented when the plasma was turned on, unfortunately, the OH flux was not guaranteed to be identical to the OD flux, which makes the determination of the accurate relative efficiencies difficult in the present study. Nevertheless, the OH and OD fluxes did not vary significantly from one another because the column densities of the reaction products, such as H₂O or H₂O₂ in the H₂O-fragment deposition, were comparable to those of the isotopic counterparts, such as D₂O and D₂O₂, in the D₂O-fragment deposition.

The reactions listed in Table 2 are divided into three groups based on the efficiency of each reaction relative to reaction (12): reactions with comparable efficiency (reactions (15), (18), and (20)), reactions one order of magnitude less efficient (reactions (16) and (17)), and reactions of undetermined efficiency (reactions (19) and (21)). For convenience, hereafter, these three groups are denoted A, B, and C, respectively. Although the difference in the barrier height (ΔE_a) among the reactions listed in Table 2 is small ($\Delta E_a < \sim 400$ K; Talukdar et al. 1996; Nguyen et al. 2011), it is remarkable that a considerable isotope

effect was clearly observed in groups A and B. The reactions differed intrinsically depending on whether the reaction involved H- or D-atom abstraction, and the effective masses were comparable within a reaction group, as shown in Table 2. The effective masses for the reactions in group B (0.90) were almost twice as large as those in group A (0.47). The inverse correlation between efficiency and the effective mass of reactions is a typical feature of quantum tunneling because the tunneling rate decreases considerably as the effective mass of a reaction increases, as expected from Equation (13).

The efficiencies of the reactions in group C can be determined from the increase in the column density of HDO or D₂O in reaction (19) or (21), respectively. The efficiency of reaction (19) could potentially be estimated in a straightforward way by calculating the column density of HDO formed through the reaction. This was not possible, however, because the OD-stretching band at 2435 cm⁻¹, which was used to calculate the HDO column densities in the present study, included a significant contribution from D₂O₂, as explained above. The efficiency of reaction (21) could potentially be estimated from the increase in the D₂O column density as a result of the reaction. The difference between the spectra of the codeposition and the D₂O-fragment deposition samples (Figure 8(b)) shows, however, that the D₂O column density did not increase; rather, it decreased with the codeposition of HD. We could not, therefore, calculate the increase in D₂O column density through reaction (21). The efficiencies of the reactions in group C were thought to be comparable to those in group B because the effective masses are identical, i.e. the reactions in group C were less efficient than those in group A. A summary of the discussion in this section is schematically illustrated in Figure 9, which clearly shows that OH and OD preferentially abstract H atom from hydrogen molecules (H₂ or HD), leading to H₂O and HDO, respectively.

4. ASTROPHYSICAL IMPLICATIONS

The present study demonstrated that reactions between OH and H₂ yield H₂O on a solid surface at 10 K, despite a large activation barrier (2100 K) for the reaction (Atkinson et al. 2004). We assume that reaction (12) occurred in previous experiments on the formation of H₂O through hydrogenation of O, O₂, or O₃ at 10 K (e.g. Miyauchi et al. 2008; Mokrane et al. 2009); however, this assumption was not extensively explored. This is the first experimental result to isolate reaction (12) and to show that reactions related to H₂ actually yielded H₂O. Although in a recent theoretical model, Das & Chakrabarti (2011) assumed that reaction (12) does not occur on grain surfaces in dense clouds because of the activation barrier, the present experimental result strongly suggests that models should include reaction (12) as the efficient route.

We propose that solid H_2O in dense molecular clouds is mostly formed by the following three surface reactions: $\text{OH} + \text{H}$ (reaction (2)), $\text{OH} + \text{H}_2$ (reaction (12)), and $\text{H}_2\text{O}_2 + \text{H}$ (reaction (5)). The main routes to the formation of H_2O in dense clouds are schematically illustrated in Figure 10. OH would be formed through hydrogenation of O atoms and/or other reactions (e.g., reaction (5)). It may be reasonable that H_2O formation through $\text{OH} + \text{H}_2$ is more efficient than reactions $\text{OH} + \text{H}$ in dense clouds where H_2 is more prevalent than H atoms among the various H-related species. Romanzin et al. (2011) also discussed the importance of reaction (12) relative to reaction (2) for the formation of H_2O in their experiments where energetic OH was produced by the hydrogenation of O_3 at 25–50 K. As for H_2O_2 , hydrogenation of O_2 is probably a unique pathway toward the production of H_2O_2 in dense clouds. O_2 could be produced by the reaction of $\text{O} + \text{O}$ on grain surfaces and/or supplied from the gas phase. The search for solid O_2 in interstellar environments is ongoing and has not been successful to date. Its presence has been suggested in previous studies (e.g., Boogert et al. 2002; Goldsmith et al. 2011). The recent detection of H_2O_2 in the cloud core ρ Oph A suggested that reaction (5) may be plausible on grain surfaces (Bergman et al. 2011). The upper limit for the H_2O_2 ice abundance relative to H_2O in several protostars and field stars was estimated based on laboratory IR spectra of $\text{H}_2\text{O}_2/\text{H}_2\text{O}$ mixed ice and was found to be $9\% \pm 4\%$ (Smith et al. 2011). In addition, laboratory experiments clearly demonstrated that H_2O formation through O_2 hydrogenation is efficient under conditions of dense molecular clouds (e.g., Miyauchi et al. 2008; Oba et al. 2009).

In addition to the main routes mentioned above, various reactions were proposed that could lead to the formation of H_2O and other species, such as H_2O_2 and OH (Table 1). These reactions were assumed to make only small contributions to the observed abundance of solid H_2O in dense clouds. For example, although hydrogenation of O_3 was proposed as an important route to the formation of solid H_2O in dense clouds in previous theoretical (Tielens & Hagen 1982) and experimental studies (Mokrane et al. 2009; Romanzin et al. 2011), we suspect that the contribution of this reaction to H_2O formation is small. O_3 formation is not favored on grain surfaces because the mobility and flux of H atoms is higher than the corresponding properties of O atoms, which prohibits formation of O_3 by consuming O atoms (reaction (1)) and/or O_2 (reaction (3)) prior to O_3 formation. Our conclusion is consistent with the theoretical model proposed by Cuppen & Herbst (2007), who estimated the efficiencies of reactions (2), (5), and (12) in dense clouds at 10 K to be 6%, 17%, and 77%, respectively.

The formation of solid HDO was experimentally demonstrated to occur in the present study. Although HDO in the solid state has been sought after, its detection has not been successful to date. An upper limit for the solid $\text{HDO}/\text{H}_2\text{O}$ ratio in some sources is available (Dartois et al. 2003; Parise et al. 2003). In the gas phase, the $\text{HDO}/\text{H}_2\text{O}$ ratios in the low-

mass protostars IRAS 16239-2422 and NGC1333-IRAS2A were found to be 0.03 (Parise et al. 2005) and 0.07 (Liu et al. 2011), respectively.

Kristensen et al. (2011) discussed the formation of H₂O, HDO, and D₂O through reactions of OH with H₂, HD, and D₂, respectively, on ice-covered dust grains in dense molecular clouds. They assumed that the reaction OH + HD is barrierless, and proposed that the H₂O and HDO form statistically in a ratio of 2:1, respectively, from the intermediate H₂DO. Based on these assumptions, this group claimed that the astronomically observed HDO/H₂O ratio could be explained according to their model; however, the reactions of OH/OD with H₂/HD/D₂ do have a barrier, as demonstrated in previous experimental and theoretical studies in the gas phase (e.g., Talukdar et al. 1996; Nguyen et al. 2011), as well as in the present study. Moreover, the present study demonstrated that the formation of HDO through the reactions of OH with HD were much less favored than the formation of H₂O, which is inconsistent with their assumptions. Our results are inconsistent with the theoretical predictions for the formation of H₂O and its isotopologues by Cazaux et al. (2010, 2011), who considered branching ratios of 1 to 1 between reactions (18) and (19) or between reactions (20) and (21).

The present experimental results demonstrate that a crucial factor for constraining the ratio of the HDO and H₂O abundances formed by reactions listed in Table 2 is the relative abundance of OH and OD in dense clouds. The following three reasons support this conclusion: first, the efficiency of H₂O formation through the reactions of OH with H₂ (reaction (12)) and HD (reaction (18)) is comparable to the efficiency of HDO formation through reactions of OD with H₂ (reaction (15)) or HD (reaction (20)). Second, the four reactions (i.e., H-atom abstraction reactions) are much more efficient than the other four reactions (i.e., D-atom abstraction reactions) (Table 2, Figure 9). Third, once solid H₂O is formed, its deuteration does not occur through H–D exchange with D atoms (Nagaoka et al. 2005) or with D₂O (Gálvez et al. 2011) at 10 K, even if D₂O ice forms successfully. Note that this prediction is only applicable to HDO and H₂O formation through reactions listed in Table 2.

If OH and OD are mainly produced by the reactions of O atoms with H and D atoms, respectively, the relative abundance of H and D atoms would be important to constrain the relative abundance of OH and OD. According to the deuterium fractionation models in the gas phase proposed by Roberts et al. (2002), the atomic D/H ratio is low ($< 10^{-4}$) during the early stages ($< 10^5$ years) of molecular cloud evolution. After 10^5 years, the ratio increases dramatically, reaching a value of ~ 0.06 after 10^6 years, which is comparable to the observed HDO/H₂O ratio shown above (Parise et al. 2005; Liu et al. 2011). If large regions of an ice mantle are produced during the later stages of molecular cloud evolution, the HDO/H₂O

ratio is expected to reach its highest value for the D/H atomic ratio, ~ 0.06 (Roberts et al. 2002). If not, other routes may contribute to the observed HDO/H₂O ratio.

The above scenario is based on an assumption that OH (OD) is produced through the reaction $O + H$ (D) on grain surfaces. Roberts et al. (2002) estimated the OD/OH ratios in their gas-phase model to be 0.093–0.358, higher than the atomic D/H ratio in the same model. The participation of gas-phase OD and OH in deuterium fractionation in water formation via surface reactions leads to D enrichment in ice, although the degree of enrichment will depend on the flux of the gas-phase OD and OH onto grains.

Further studies are required to inclusively discuss the formation of solid H₂O and HDO in dense molecular clouds. In future studies, care should be taken when considering chemical reactions, particularly quantum tunneling reactions, with comparable activation barriers because the reaction efficiency can differ dramatically among such reactions, as clearly demonstrated in the present study.

This work was partly supported by a Grant-in-Aid for Scientific Research from the Japan Society for the Promotion of Science (JSPS) and by a research fellowship from JSPS for Young Scientists (Y.O.).

REFERENCES

- Alagia, M., Balucani, N., Casavecchia, P., Stranges, D., & Volpi, G. 1993, *J. Chem. Phys.*, 98, 2459
- Atkinson, R., et al. 2004, *Atmos. Chem. Phys.*, 4, 1461
- Baulch, D. L. et al. 1992, *J. Phys. Chem. Ref. Data*, 21, 411
- Bergman, P., Parise, B., Liseau, R., Larsson, B., Olofsson, H., Menten, K. M., & Gusten, R. 2011, *A&A*, 531, L8
- Boogert, A. C. A., Blake, G. A., & Tielens, A. G. G. M. 2002, *ApJ*, 577, 271
- Cazaux, S., Caselli, P., & Spaans, M. 2011, *ApJ*, 741, L34
- Cazaux, S., Cobut, V., Marseille, M., Spaans, M., & Caselli, P. 2010, *A&A*, 522, A74
- Chu, L., & Anastasio, C. 2005, *J. Phys. Chem. A* 109, 6264

- Cuppen, H. M., Ioppolo, S., Romanzin, C., & Linnartz, H. 2010, *Phys. Chem. Chem. Phys.*, 12, 12077
- Cuppen, H. M., & Herbst, E. 2007, *ApJ*, 668, 294
- Dartois, E., Thi, W.-F., Geballe, T. R., Deboffle, D., d’Hendecourt, L., & van Dishoeck, E. 2003, *A&A*, 399, 1009
- Das, A., & Chakrabarti, S. K. 2011, *Mon. Not. R. Astron. Soc.*, 418, 545
- de Beer, E., Koopmans, M. P., de Lange, C. A., Wang, Y., & Chupka, W. A. 1991, *J. Chem. Phys.*, 94, 7634
- Devlin, J. P., Wooldridge, P. J., & Ritzhaupt, G. 1986, *J. Chem. Phys.*, 84, 6095
- Dieke, G. H., & Crosswhite, H. M. 1962, *J. Quant. Spectrosc. Radiat. Transf.*, 2, 97
- Dulieu, F., et al. 2010, *A&A*, 512, A30
- Gálvez, Ó., Maté, B., Herrero, V. J., & Escribano, R. 2011, *ApJ*, 738, 133
- Gerakines, P. A., Schutte, W. A., Greenberg, J. M., & van Dishoeck, E. F. 1995, *A&A*, 296, 810
- Goldsmith, P. F. et al. 2011, *ApJ*, 737, 96
- Greenslade, M. E., Lester, M. I., Radenovic, D. C., van Rooij, A. J. A., & Parker, D. H. 2005, *J. Chem. Phys.*, 123, 074309
- Hama, T., Watanabe, N., Kouchi, A., & Yokoyama, M. 2011, *ApJ*, 738, L15
- Hasegawa, T. I., Herbst, E., & Leung, C. M. 1992, *ApJS*, 82, 167
- Hidaka, H., Kouchi, A., & Watanabe, N. 2007, *J. Chem. Phys.* 126, 204707
- Hidaka, H., Watanabe, M., Kouchi, A., & Watanabe, N. 2009, *ApJ*, 702, 291
- Hiraoka, K., Miyagoshi, T., Takayama, T., Yamamoto, K., & Kihara, Y. 1998, *ApJ*, 498, 710
- Hornig, D. F., White, H. F., & Reding, R. P. 1958, *Spectrochim. Acta*, 12, 338
- Hoshina, H., Fushitani, M., Momose, T., & Shida, T. 2004, *J. Chem. Phys.*, 120, 3706
- Huber, K. P., & Herzberg, G. 1979, *Molecular Spectra and Molecular Structure IV. Constants of Diatomic Molecules* (Van Nostrand Reinhold, New York)

- Ikawa, S., & Maeda, S. 1968, *Spectrochim. Acta*, 24A, 655
- Ioppolo, S., Cuppen, H. M., Romanzin, C., van Dishoeck, E. F., & Linnartz, H. 2008, *ApJ*, 686, 1474
- Jing, D., He, J., Brucato, J., De Sio, A., Tozzetti, L., & Vidali, G. 2011, *ApJ*, 741, L9
- Johnston, H. S. 1966, *Gas Phase Reaction Rate Theory*, ed. B. Crawford Jr., W. D. McElroy, & C. C. Price (New York: Roland), 51
- Keyser, L. F. 1979, *J. Phys. Chem.*, 83, 645
- Keyser, L. F. 1986, *J. Phys. Chem.*, 90, 2994
- Kobayashi, K. 1983, *J. Phys. Chem.*, 87, 4317
- Kohno, N., Izumi, M., Kohguchi, H., & Yamasaki, K. 2011, *J. Phys. Chem. A*, 115, 4867
- Koussa, H., Bahri, M., Jaidan, N., & Lakhdar, Z. B. 2006, *J. Mol. Struct.: THEOCHEM*, 770, 149
- Krasnoperov, L. N., & Michael, J. V. 2004, *J. Phys. Chem. A*, 108, 5643
- Kristensen, L. E., Amiaud, L., Fillion, J.-H., Dulieu, F., & Lemaire, J.-L. 2011, *A&A*, 527, A44
- Lannon, J. A., Verderame, F. D., & Anderson, R. W. Jr. 1971, *J. Chem. Phys.*, 54, 2212
- Liu, F.-C., Parise, B., Kristensen, L., Visser, R., van Dishoeck, E. F., & Gusten, R. 2011, *A&A*, 527, A19
- Miyauchi, N., Hidaka, H., Chigai, T., Nagaoka, A., Watanabe, N., & Kouchi, A. 2008, *Chem. Phys. Lett.*, 456, 27
- Mokrane, H., Chaabouni, H., Accolla, M., Congiu, E., Dulieu, F., Chehrouri, M., & Lemaire, J. L. 2009, *ApJ*, 705, L195
- Momose, T., Hoshina, H., Sogoshi, N., Katsuki, H., Wakabayashi, T., & Shida, T. 1998, *J. Chem. Phys.*, 108, 7334
- Mousavipour, S. H., & Saheb, V. 2007, *Bull. Chem. Soc. Jpn.*, 80, 1901
- Nagaoka, A., Watanabe, N., & Kouchi, A. 2005, *ApJ*, 624, L29
- Nagaoka, A., Watanabe, N., & Kouchi, A. 2007, *J. Phys. Chem. A*, 111, 3016

- Nguyen, T. L., Stanton, J. F., & Barker, J. R. 2011, *J. Phys. Chem. A*, 115, 5118
- Oba, Y., Miyauchi, N., Hidaka, H., Chigai, T., Watanabe, N., & Kouchi, A. 2009, *ApJ*, 701, 464
- Oba, Y., Watanabe, N., Kouchi, A., Hama, T., & Pirronello, V. 2010a, *ApJ*, 712, L174
- Oba, Y., Watanabe, N., Kouchi, A., Hama, T., & Pirronello, V. 2010b, *ApJ*, 722, 1598
- Oba, Y., Watanabe, N., Kouchi, A., Hama, T., & Pirronello, V. 2011, *Phys. Chem. Chem. Phys.*, 13, 15792
- Oldenberg, R. C., Loge, G. W., Harradine, D. M., & Winn, K. R. 1992, *J. Phys. Chem.*, 96, 8426
- Orkin, V. L., Kozlov, S. N., Poskrebyshv, G. A., & Kurylo, M. J. 2006, *J. Phys. Chem. A*, 110, 6978
- Parise, B., Simon, T., Caux, E., Dartois, E., Ceccarelli, C., Rayner, J., & Tielens, A. G. G. M. 2003, *A&A*, 410, 897
- Parise, B. et al. 2005, *A&A*, 431, 547
- Ravishankara, A. R., Nicovich, J. M., Thompson, R. L., & Tully, F. P. 1981, *J. Phys. Chem.*, 85, 2498
- Roberts, H., Herbst, E., & Millar, T. J. 2002, *Mon. Not. R. Astron. Soc.*, 336, 283
- Romanzin, C., Ioppolo, S., Cuppen, H. M., van Dishoeck, E. F., & Linnartz, H. 2011, *J. Chem. Phys.* 134, 084504
- Sellevag, S. R., Georgievskii, Y., & Miller, J. A. 2008, *J. Phys. Chem. A*, 112, 5085
- Smith, R. G., Sellgren, K., & Tokunaga, A. T. 1989, *ApJ*, 344, 413
- Smith, R. G., Charnley, S. B., Pendleton, Y. J., Wright, C. M., Maldoni, M. M., & Robinson, G. 2011, *ApJ*, 743, 131
- Talukdar, R. K., Gierczak, T., Goldfarb, L., Rudich, Y., Madhava Rao, B. S., & Ravishankara, A. R. 1996, *J. Phys. chem.*, 100, 3037
- Tielens, A. G. G. M. 2005, *The Physics and Chemistry of the Interstellar Medium* (Cambridge: Cambridge Univ. Press)
- Tielens, A. G. G. M., & Hagen, W. 1982, *A&A*, 114, 245

- Timmermans, E. A. H., et al. 1998, *Spectrochim. Acta B*, 53, 1553
- Timmermans, E. A. H., et al. 1999, *Spectrochim. Acta B*, 54, 1085
- Tsang, W., & Hampson, R. F. 1986, *J. Phys. Chem. Ref. Data*, 3, 1087
- Vaghjiani, G. L., Ravishankara, A. R., & Cohen, N. 1989, *J. Phys. Chem.*, 93, 7833
- Walch, S. P., Rohlfiing, C. M., Melius, C. F., Bauschlicher, C. W. Jr 1988, *J. Chem. Phys.*, 88, 6273
- Watanabe, N., & Kouchi, A., 2008, *Prog. Surf. Sci.*, 83, 439
- Watanabe, N., Nagaoka, A., Hidaka, H., Shiraki, T., Chigai, T., & Kouchi, A. 2006, *Planet. Space Sci.*, 54, 1107
- Watanabe, N., Kimura, Y., Kouchi, A., Chigai, T., Hama, T., & Pirronello, V. 2010, *ApJ*, 714, L233
- Zins, E.-L., Joshi, P. R., & Krim, L. 2011, *Mon. Not. R. Astron. Soc.*, 415, 3107

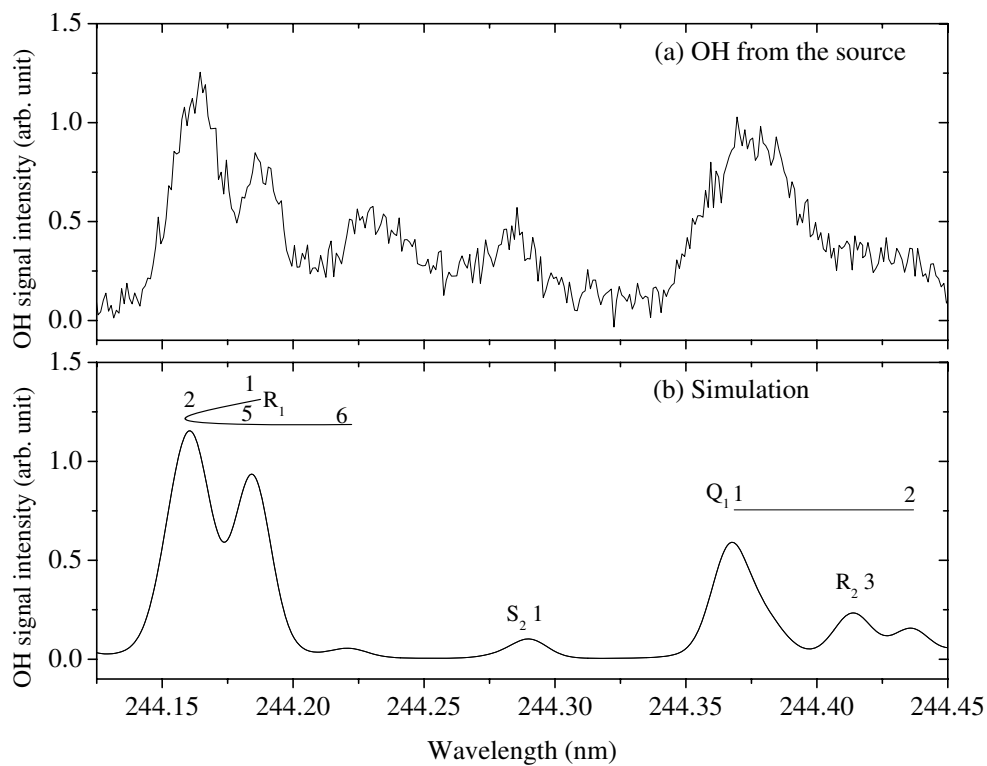


Fig. 1.— (a) $(2 + 1)$ REMPI spectrum of OH emitted from the radical source through the Al pipe at room temperature and (b) the best-fit simulated spectrum for $T_{\text{rot}} = 300$ K. The capital numbers 1–6 indicate rotational levels of Q, R, and S branches associated with the $X^2\Pi$ ground state of OH. The subscript numbers 1 and 2 represent the lower or upper members of the rotational level in the $X^2\Pi$ ground state, respectively, because spin-orbit coupling causes the rotational levels to split into two components (de Beer et al. 1991; Dieke & Crosswhite 1962).

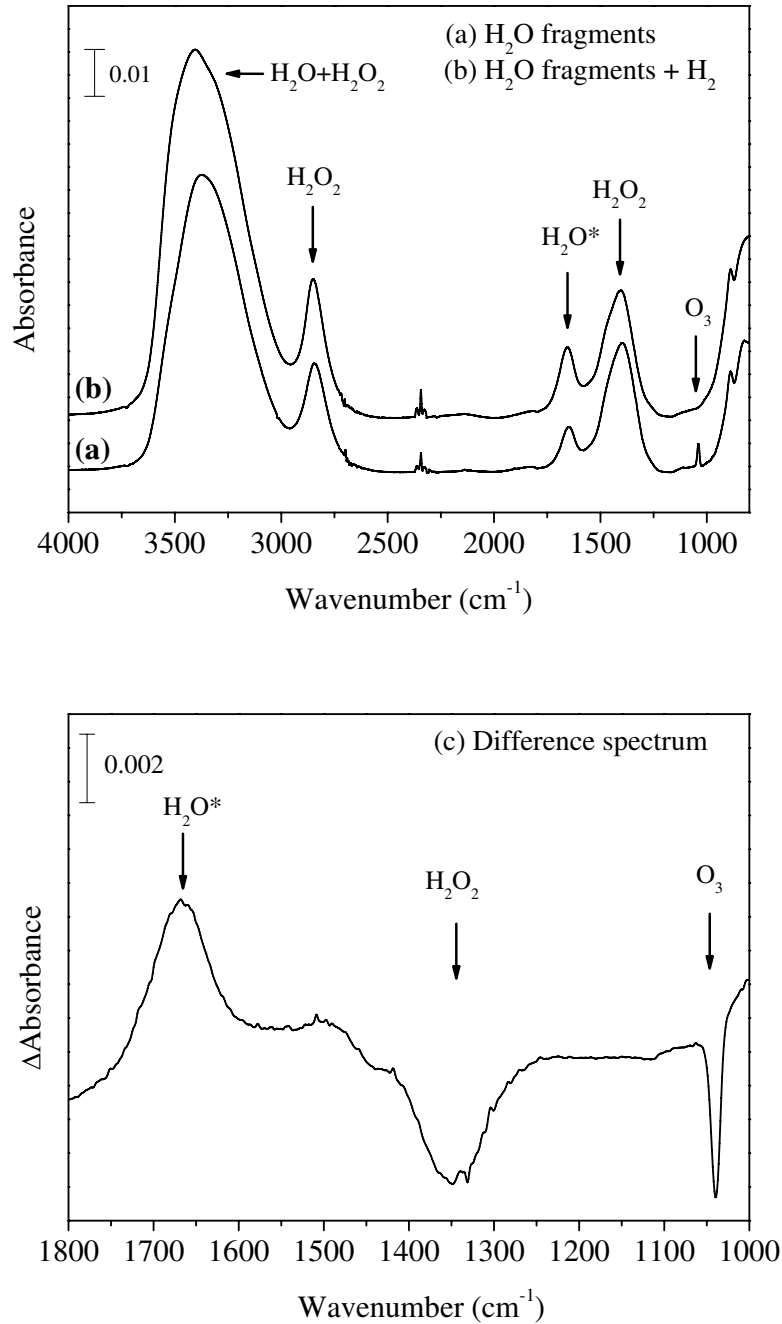


Fig. 2.— FTIR spectra after (a) deposition of H₂O fragments and (b) codeposition of H₂O fragments with H₂. (c) The spectral differences relative to the H₂O-fragment deposition sample. The peak with the asterisk (*) was used for quantification purposes. The peaks at ~2300 cm⁻¹ and ~2700 cm⁻¹ were derived from the background CO₂ and the inherent noises caused by vibration of the He refrigerator, respectively.

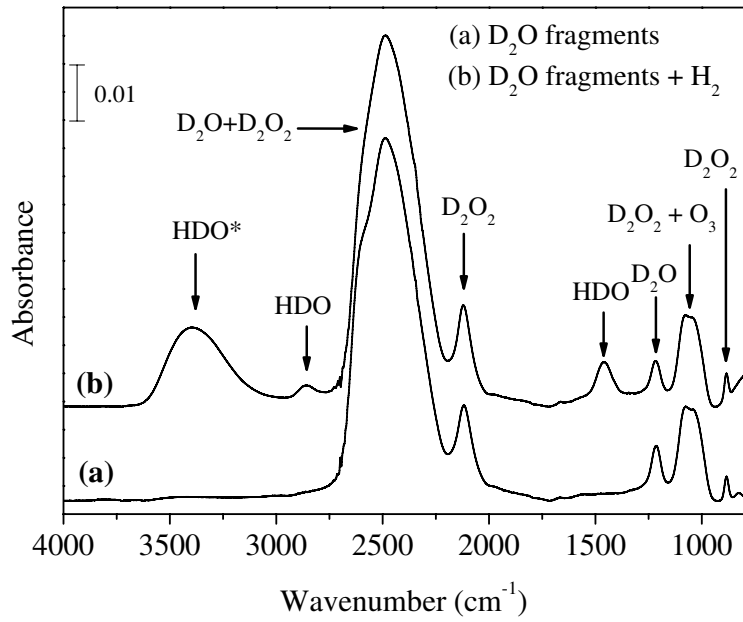


Fig. 3.— FTIR spectra after (a) deposition of D₂O fragments and (b) codeposition of D₂O fragments with H₂. The peak with the asterisk (*) was used for quantification purposes.

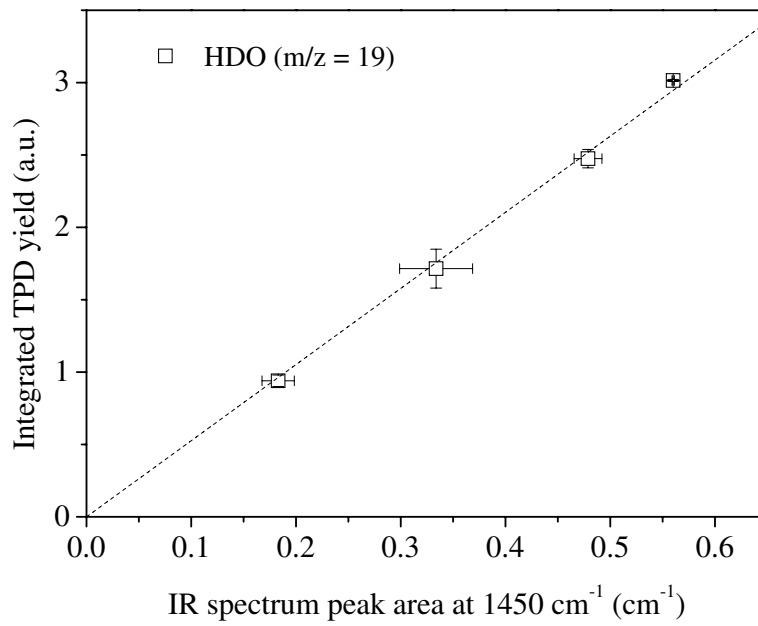


Fig. 4.— Integrated TPD yield of HDO ($m/z = 19$) as a function of the IR peak area of the 1450 cm^{-1} band, which appeared upon the codeposition of D_2O fragments with H_2 . The data points show the averaged values with statistical errors for four different durations. A dashed line represents the best-fitting straight line through the points.

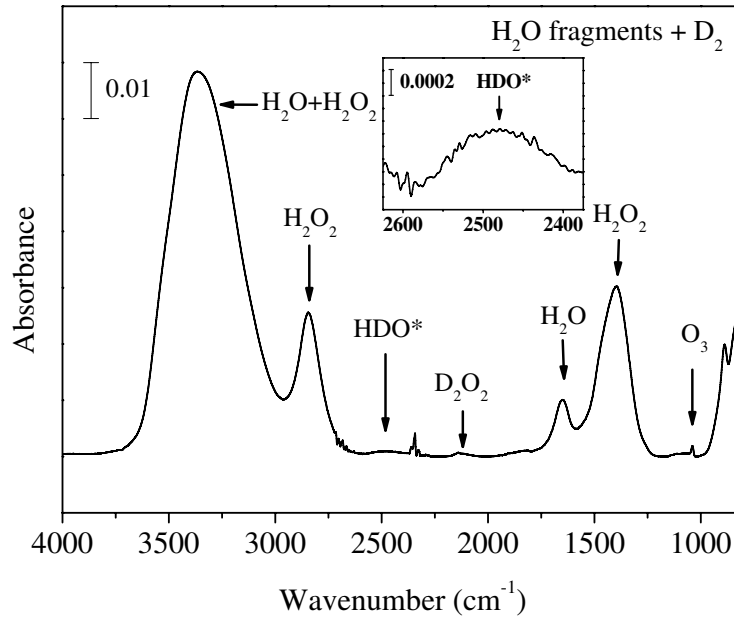


Fig. 5.— FTIR spectrum after codeposition of H₂O fragments with D₂. The peak with the asterisk (*) was used for quantification purposes. The inset shows the OD-stretching band of HDO at 2475 cm⁻¹.

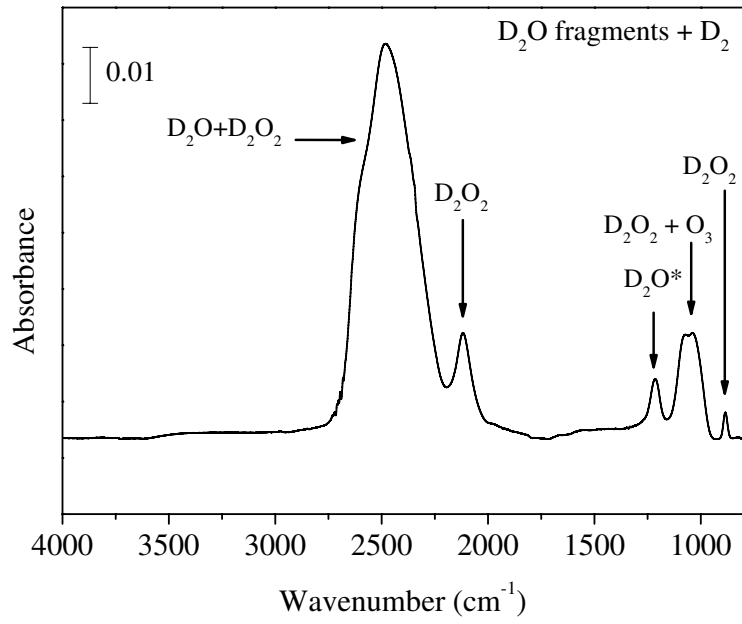


Fig. 6.— FTIR spectrum after codeposition of D₂O fragments and D₂. The peak with the asterisk (*) was used for quantification purposes.

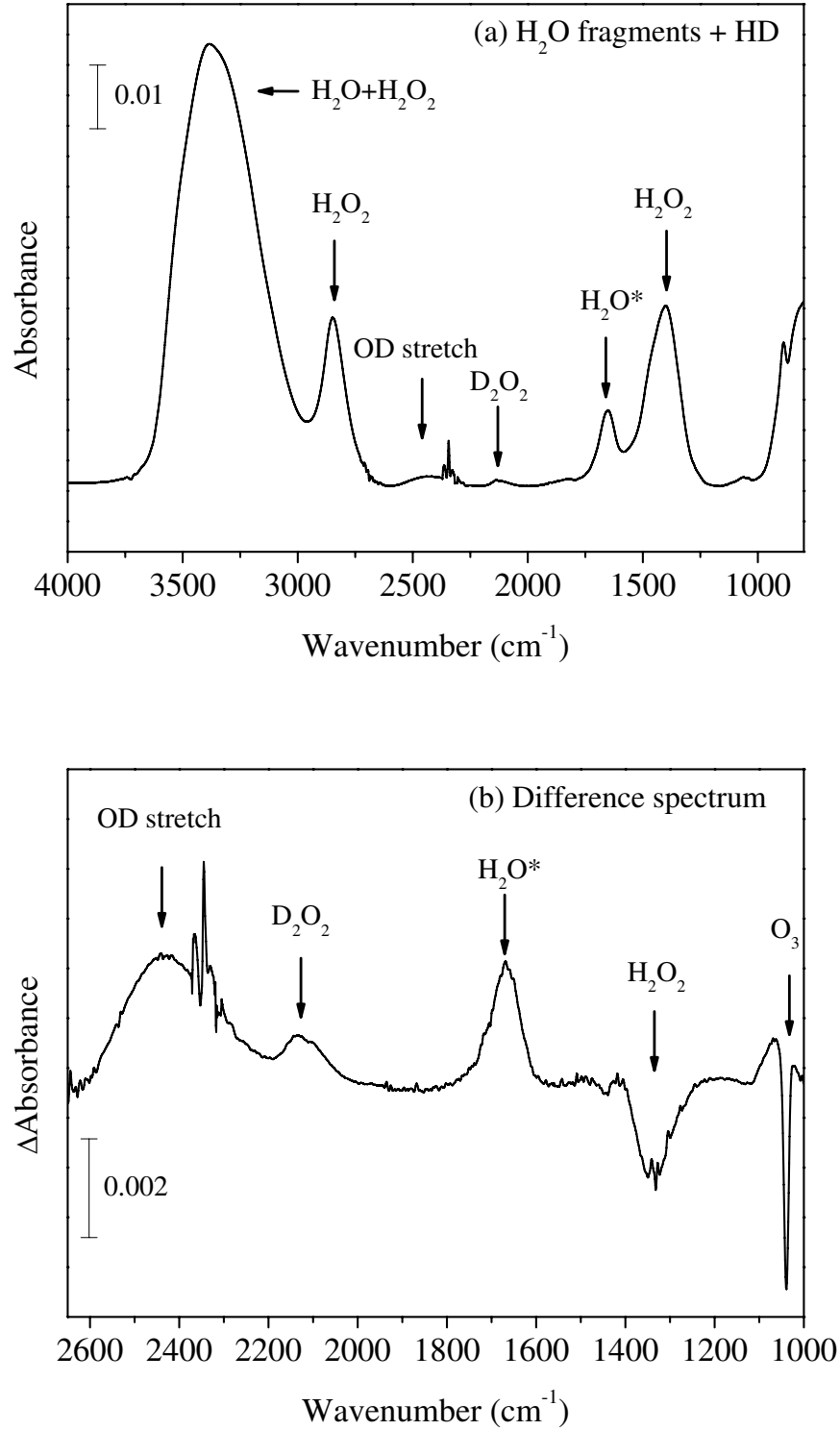


Fig. 7.— (a) FTIR spectrum after codeposition of H₂O fragments with HD and (b) the spectral differences relative to the H₂O-fragment deposition sample. The peak with the asterisk (*) was used for quantification purposes. The peaks at 2300 cm⁻¹ were derived from the background CO₂.

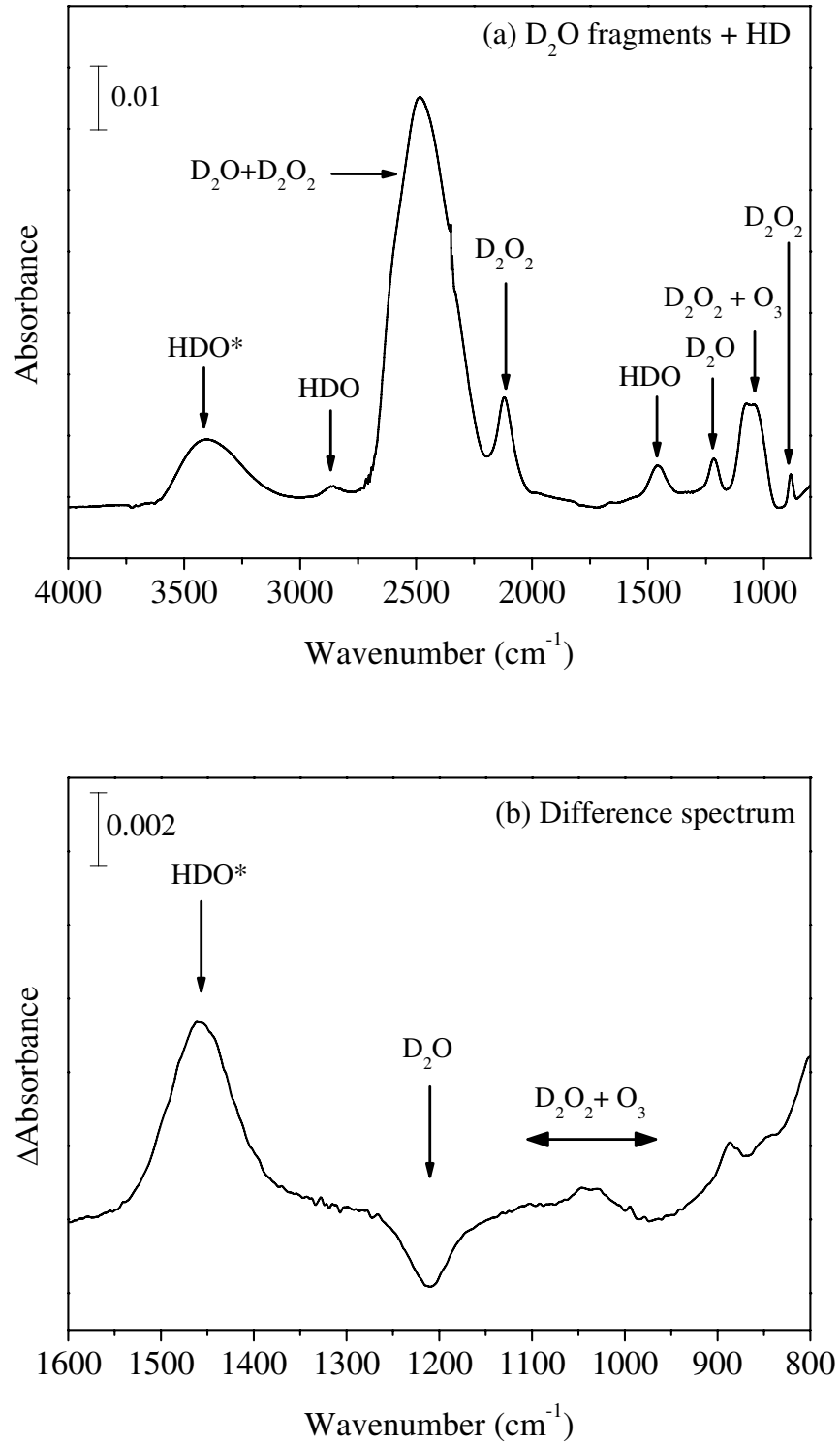


Fig. 8.— (a) FTIR spectrum after the codeposition of D_2O fragments with HD and (b) the spectral differences relative to the D_2O -fragment deposition sample. The peak with the asterisk (*) was used for quantification purposes.

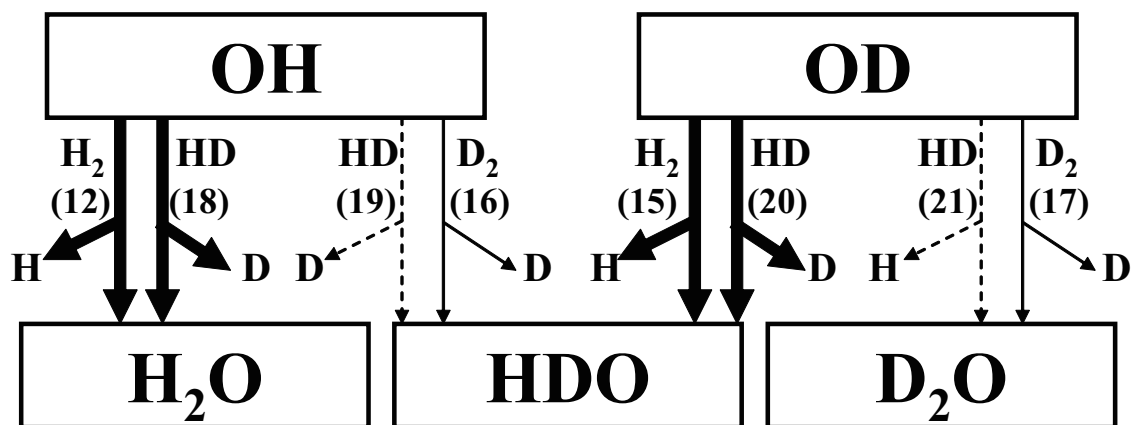


Fig. 9.— Schematic illustration showing the reaction network for the formation of solid H₂O and its isotopologues (HDO and D₂O) via the reactions listed in Table 2. The broad or narrow lines represent reactions with relative efficiencies of about 1 or 0.1, respectively, compared to reaction (12) (Table 2). The dashed lines indicate reactions with efficiencies that could not be estimated experimentally. The numbers correspond to the reaction numbers given in the text and Table 2. This figure clearly shows that OH and OD preferentially abstract H atom from hydrogen molecules (H₂ or HD), leading to H₂O and HDO, respectively.

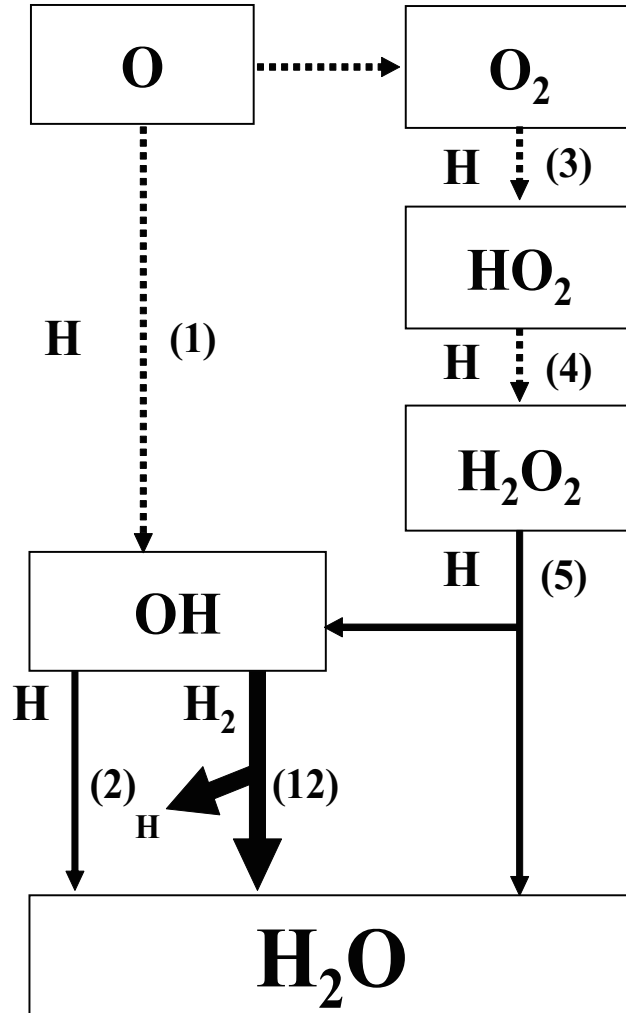


Fig. 10.— Main routes to the formation of solid H_2O in dense molecular clouds: hydrogenation of OH (reaction (2)), the reaction of OH with H_2 (reaction (12)), and the reaction of H_2O_2 with H atom (reaction (5)), which are denoted by solid lines. Other reactions are denoted by dotted lines. The title reaction $\text{OH} + \text{H}_2$ is denoted by a thick line. The numbers in parentheses correspond to the reaction numbers given in the text and Table 1.

Table 1. Surface reactions proposed for the formation of solid H₂O and the related species

Number	Reaction	E_a (K)	ΔH° (kJ mol ⁻¹)	Reference
1	O + H → OH	0	-429	
2	OH + H → H ₂ O	0	-499	
3	O ₂ + H → HO ₂	~0	-203	a
4	HO ₂ + H → H ₂ O ₂	0	-354	b
5	H ₂ O ₂ + H → H ₂ O + OH	2000	-285	c
6	OH + OH → H ₂ O ₂	0	-211	d
7	OH + OH → H ₂ O + O	0	-71	d
8	HO ₂ + H → H ₂ OO* → H ₂ O + O(¹ D)	0	-10 ^h	b
9	HO ₂ + H → H ₂ O..O → H ₂ O + O(³ P)	9300	-242	b
10	HO ₂ + H → H ₂ + O ₂ (³ Σ _g ⁻)	750	-229	b
11	O ₃ + H → OH + O ₂	500	-321	e
12	OH + H ₂ → H ₂ O + H	2100	-62	d
22	O + H ₂ → OH + H	3160	+8	f
23	HO ₂ + H ₂ → H ₂ O ₂ + H	13100	+58	g

^aWalch et al. (1988); Sellevag et al. (2008).

^bMousavipour & Saheb (2007).

^cKoussa et al. (2006).

^dAtkinson et al. (2004).

^eKeyser (1979).

^fBaulch et al. (1992).

^gTsang & Hampson (1986).

^hThis reaction as a whole is exothermic; however, the latter part of the reaction (H₂OO* → H₂O + O(¹D)) is endothermic by 151 kJ mol⁻¹.

Note. — ΔH° denotes the experimental enthalpy change for the gas-phase reactions in kJ mol⁻¹, where 1 kJ mol⁻¹ corresponds to 120 K. Values of E_a and ΔH° are derived from gas-phase reactions.

Table 2. Summary of the Activation Barrier (K), the Effective Mass, and the Measured Efficiency for Reactions OH + H₂ and the Isotopologues.

Number	Reaction	Section ^a	^b	^c E_a (K)	^d	Atom Abstracted	Effective Mass ^e	Relative Efficiency ^f
12	OH + H ₂ → H ₂ O + H	3.1	2000	2100	2935	H	0.47	1
15	OD + H ₂ → HDO + H	3.2			2789	H	0.48	~1
16	OH + D ₂ → HDO + D	3.3	2456		3026	D	0.90	~0.1
17	OD + D ₂ → D ₂ O + D	3.4			2870	D	0.91	~0.1
18	OH + HD → H ₂ O + D	3.5	2130		2855	H	0.48	~1
19	OH + HD → HDO + H	3.5	2130		3051	D	0.90	n.d. ^g
20	OD + HD → HDO + D	3.5			2703	H	0.48	~1
21	OD + HD → D ₂ O + H	3.5			2900	D	0.90	n.d. ^g

^aA corresponding section in the present paper.

^bExperimentally determined values (Talukdar et al. 1996).

^cCompilation of literature values (Atkinson et al. 2004).

^dComputed reaction barrier heights including harmonic zero-point vibrational energy (Nguyen et al. 2011).

^eCalculated by using Equation (14) (Johnston 1966).

^fEstimated by comparison of the yield of the product (H₂O, HDO, or D₂O) for each reaction with that of H₂O for reaction (12).

^gNot determined due to reasons described in the text.